Coherent control of cold-molecule formation through photoassociation using a chirped-pulsed-laser field

J. Vala,[1] O. Dulieu,[2] F. Masnou-Seeuws,[2] P. Pillet,[2] and R. Kosloff[1]
[1]*Department of Physical Chemistry and the Fritz Haber Research Center for Molecular Dynamics, the Hebrew University, 91904 Jerusalem, Israel*
[2]*Laboratoire Aimé Cotton, CNRS II, Bâtiment 505, Campus d'Orsay, F91405 Orsay Cedex, France*
(Received 19 April 2000; published 12 December 2000)

Enhancement of the production of cold molecules via photoassociation is considered for the Cs_2 system. The employment of chirped picosecond pulses is proposed and studied theoretically. The analysis is based on the ability to achieve impulsive excitation which is given by the ultracold initial conditions where the nuclei are effectively stationary during the interaction with a field. The appropriate theoretical framework is the coordinate-dependent two-level system. Matching the pulse parameters to the potentials and initial conditions results in full Rabi cycling between the electronic potentials. By chirping the laser pulse, adiabatic transfer leading to the population inversion from the ground to the excited state is possible in a broad and tunable range of internuclear distance. Numerical simulations based on solving the time-dependent Schrödinger equation (TDSE) were performed. The simulation of the photoassociation of Cs_2 from the ground $^3\Sigma_u^+$ to the excited 0_g^- state under ultracold conditions verifies the qualitative picture. The ability to control the population transfer is employed to optimize molecular formation. Transfer of population to the excited 0_g^- surface leaves a void in the nuclear density of the ground $^3\Sigma_u^+$ surface. This void is either filled by thermal motion or by quantum ''pressure'' and it is the rate-determining step in the photoassociation. The spontaneous-emission process leading to cold-molecules is simulated by including an optical potential in the TDSE. Consequently, the rate of cold molecule formation in a pulsed mode is found to be larger than that obtained in a continuous-wave mode.

DOI: 10.1103/PhysRevA.63.013412 PACS number(s): 32.80.Qk, 33.80.Ps, 33.80.Be

I. INTRODUCTION

The physics of dilute gases has seen major progress in two fields: laser cooling of atomic samples and coherent control. In both cases, a strong motivation is to use laser light in order to achieve control of the system leading it to a desired final state.

Among the many applications of cold atoms, the photoassociation reaction, where two atoms absorb a photon to create an excited molecule, is a very important one. It has been proposed by Thorsheim *et al.* [1] and observed for all homonuclear alkali-metal dimers. Photoassociation was first achieved in a sodium cold atomic sample [2–4], then in rubidium [5,6], in lithium [7], in potassium [8], and finally in cesium [9,10]. Besides, the photoassociation reaction has been studied in a sample of metastable helium atoms [11] and of hydrogen [12]. Effort has also been devoted to photoassociating two different alkali-metal atoms [13,14]. Most experiments were performed with continuous lasers, harvesting a variety of accurate molecular spectroscopy data.

Furthermore, recent observation of ground-state ultracold molecules obtained by spontaneous radiative decay of photoassociated molecules [9,15,16] is opening a new research field. Theoretical investigation of the photoassociation process has been performed mainly in the framework of a time-independent approach [17–20] using a perturbative treatment. In the framework of the Franck-Condon picture, the photoassociation rate is computed as a vertical transition between the continuum state of two colliding distant atoms and the long-range vibrational state of an excited molecule, with a wave function approximated by an Airy function at the outer turning point. This picture is confirmed by experimental observation, where modulations in the photoassociation rate as a function of laser detuning faithfully reflect the nodal structure of the ground-state wave function [21]. Besides these modulations, a simple analytical formula [19] predicts for J-wave scattering a temperature dependence in T^{J-1}, an intensity dependence in I, with a $\Delta^{-(4J+7)/6}$ variation as a function of the detuning Δ. At low laser intensities, such a simple model is in good qualitative agreement with the experimental observations [22]. Similar estimations were obtained in the quasicontinuum modeling of Ref. [23]. We should note that the dependence upon the detuning can be physically interpreted as absorption of a photon by a pair of atoms standing still at a distance R such that the asymptotic potential $-C_3/R^3$ is equal to the detuning.

The investigation of the ultracold molecules strongly depends on the yield of the photoassociation process. The purpose of this study is to explore the possibility of employing a coherent manipulation technique to optimize the photoassociation yield. To gain insight into the control scheme one has to bridge the conceptual gap between time dependent light induced manipulations and the well established continuous-wave (CW) photoassociation spectroscopy.

The crucial step in the process is to optically pump population from the unbound ground electronic surface to a bound excited one. Taking advantage of the special conditions of ultracold collisions, it is relatively easy to reach the situation where the nuclei are stationary for the period of the pulse excitation. For molecules at normal temperatures, these con-

ditions translate to impulsive excitation in the ultrafast time domain. This has been demonstrated in the ultrafast photoassociation of mercury [24–26].

Manipulating the temporary shape of the pulse is a common endeavor in the ultrafast regime. For example, the yield of a photodissociation reaction has been manipulated experimentally by shaping the phase of the laser pulse [27]. The most simple coherent manipulation which controls the transfer of population from one electronic state to another is to linearly chirp the excitation pulse [28]. This fact has initiated a vast amount of activity in the employment of such pulses for coherent control [29–32]. The obvious advantage of a manipulation technique of this type is its experimental feasibility.

The present study follows a suggestion by Cao, Bardeen, and Wilson [33], showing that the photoexcitation yield can be made complete by creating adiabatic following conditions, simply by chirping the excitation pulse. In the case prevailing in ultracold photoassociation processes, the conditions for adiabatic following are even more favorable. The collisions are so slow that even for pulses in the picosecond time scale, the nuclei are practically frozen. As a result, one can decompose the process into a stationary ensemble of coordinate-dependent two-level systems. In this picture, the adiabatic following ideas presented by Eberly [34,35] can be employed leading to a complete and robust population transfer.

The content of the paper starts in Sec. II with a general description of the process of interest and tools for treating it. This is followed in Sec. III by a discussion of various models describing the light–cold-molecule interaction with special emphasis on a chirped pulsed field. In Sec. IV, we discuss cesium photoassociation using a chirped pulsed field. The cold-molecule formation process including a discussion of spontaneous emission is treated in Sec. V.

II. SYSTEM OF INTEREST

The process studied is the formation of a translationally cold cesium dimer in the lowest triplet state from a cloud of cesium atoms cooled to a temperature of 200 μK. As schematically illustrated in Fig. 1, the process consists of two steps. The first one, which we particularly focus on, is photoassociation of two cesium atoms moving on the $^3\Sigma_u^+(6s+6s)$ potential to the cesium dimer in the excited 0_g^- $(6s+6p_{3/2})$ molecular state. The time scale of the long-range vibrational motion of these molecules is typically in units of nanoseconds. The second step is the spontaneous-emission decay of the excited population to the bound levels of the electronic ground-state potential forming the stable translationally cold cesium molecule. The double-well topology of the 0_g^- potential favors this process. The potential barrier has a slow R^{-3} variation, locally enhancing the probability density of the vibrational wave functions and, hence, their Franck-Condon overlap with the vibrational eigenfunctions of the ground electronic potential. Recently, the enhancement of the spontaneous decay to triplet molecular states by single-channel and multichannel tunneling was considered [36].

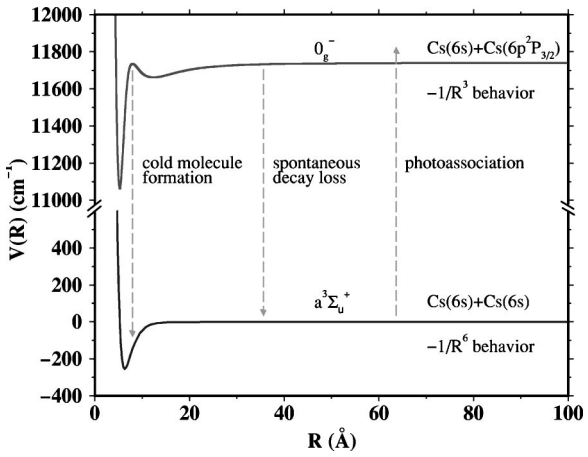

FIG. 1. The formation of the ultracold cesium dimer in $^3\Sigma_u^+$ through photoassociation onto the long-range 0_g^- molecular state followed by the spontaneous decay to the vibrational levels of the lowest triplet state.

Construction of the 0_g^- potential curve is described by Fioretti *et al.* [10] in detail. Briefly, *ab initio* short-range [37] and long-range [38] curves in Hund's case (a) representation are first matched around 26 a.u., after which the atomic spin-orbit interaction is diagonalized to obtain the 0_g^- state.

The long-range part of the potential curves behaves according to the following formulas (in atomic units):

$$V_{^3\Sigma_u^+}(R) = -\frac{C_6}{R^6} - \frac{C_8}{R^8} - \frac{C_{10}}{R^{10}}, \tag{2.1}$$

where $C_6 = 6.331 \times 10^{-3}$, $C_8 = 9.63 \times 10^{-5}$, $C_{10} = 15.2 \times 10^{-7}$, and

$$V_{0_g^-}(R) = -\frac{D_3}{R^3} - \frac{2D_3^2}{\Delta E_{\rm fs} R^6}, \tag{2.2}$$

where $D_3 = 10.47$ and $\Delta E_{\rm fs}$ is the fine-structure splitting [10].

A. Initial state

The photoassociation process is conducted in a gas of cold atoms, initially at thermal equilibrium. The temperatures and densities are such that a Maxwell-Boltzmann distribution can be employed. The mean interatomic distance is approximately two orders of magnitude larger than the thermal wavelength of the particles. Characteristics of the distribution of a gas of alkali-metal atoms are summarized in Table I.

The state of a colliding pair is represented by a thermal density operator. Since only the relative motion of a pair of atoms is involved, the center-of-mass motion can be eliminated. Using relative coordinates, the state of the ensemble becomes $\hat{\rho} = \exp(-\beta \hat{\mathbf{H}})/Z$, where $\hat{\mathbf{H}}$ is the internal Hamiltonian of the colliding pair and Z is the partition function. For low gas density, the small intermolecular interaction region can be ignored leading to $\rho \approx \exp(-\beta \hat{\mathbf{T}})/Z$, where $\hat{\mathbf{T}}$ is

TABLE I. Characteristics of the Maxwell-Boltzmann distribution of a gas of alkali-metal atoms corresponding to a temperature of 200 μK. The particle density 10^{11} cm^{-3} gives the mean interatomic distance $\overline{d}$ to be 2.15 μm. The minimal uncertainty of the internuclear distance, ΔR, is given by the momentum uncertainty of the atomic relative motion Δp_{rel}.

	Li	Na	K	Rb	Cs
M (a.m.u.)	6.94	22.98	39.10	85.47	132.91
λ (nm)	67.8	37.3	28.6	19.3	15.5
$\overline{d}/\lambda$	32	58	75	112	140
$\overline{v_{\mathrm{rel}}}$ (m s^{-1})	1.105	0.607	0.465	0.315	0.252
Δp_{rel} ($\times 10^{27}$ kg m s^{-1})	2.69	4.88	6.36	9.44	11.80
ΔR (nm)	19.6	10.81	8.29	5.59	4.47

the kinetic-energy operator and $\beta = 1/k_B T$. The next step is to represent the kinetic energy operator in radial and angular coordinates. For a sufficiently cold ensemble of molecules, only s waves are usually considered, reducing further the description of the radial coordinate. However, as long as the photoassociation process takes place at longer internuclear distance, also higher angular momentum states should be considered [39]. The contribution of these states is discussed later.

For s waves, the density operator, diagonal in the radial momentum representation, can be decomposed to a set of Gaussian wave-packet projections whose width is determined by the momentum spread in the Maxwell-Boltzmann distribution and which are uniformly distributed along the internuclear distance:

$$\hat{\rho}_S(\beta) = C \int_{R_0}^{\infty} |\Psi(\beta,r)\rangle\langle\Psi(\beta,r)| r^2 dr, \tag{2.3}$$

where C is a normalization constant and $\Psi(\beta,r)$ is a thermal wave packet defined as

$$\Psi(\beta,r) = \frac{1}{r}\psi(\beta,r) = \frac{1}{r} e^{-[(R-r)^2/2\sigma^2] + ikR}. \tag{2.4}$$

The width σ is determined by the temperature $\sigma \approx \sqrt{\beta/4\mu}$. In the following section, the photoassociation dynamics of a single initial wave packet, described by Eq. (2.4), will be studied.

For extremely low temperatures, the assumption that the thermal density is dominated by the kinetic energy is not valid. The low-energy eigenfunctions in the continuum have a common stationary phase point at the outer region of the potential, which results in a strong modulation of the initial density. This qualitative picture was studied for cesium in the lowest triplet state and a temperature of 200 μK by calculating the atomic distribution along the internuclear distance. This was carried out by a Boltzmann-weighting of the density composed from individual continuum wave functions in a large range of energy and angular momentum. The continuum wave functions were calculated by the mapped Fourier grid method of Kokoouline *et al.* [40,41]. The calculations of the initial density operator were able to reproduce the modulations of the photoassociation spectra obtained by Fioretti *et al.* [10].

It was found that the last node of the atomic distribution is positioned below the internuclear distance of 50 Å. The distribution is approximately uniform above this value. Since the typical range of internuclear coordinate considered in the present study is larger than 100 Å, the decomposition of the density operator into projectors composed of thermal Maxwell-Boltzmann Gaussian wave packets is justified. The initial state has to be modified for lower temperatures and large detuning, for which photoassociation is achieved at smaller internuclear distances.

B. The Hamiltonian operator

The Hamiltonian of the system generates the dynamics of a pair of atoms moving on two electronic surfaces coupled by an electromagnetic field:

$$\hat{\mathbf{H}} = \hat{\mathbf{H}}_g \otimes \hat{\mathbf{P}}_g + \hat{\mathbf{H}}_e \otimes \hat{\mathbf{P}}_e + \hat{\mathbf{W}}(t) \otimes \hat{\mathbf{S}}_x = \begin{pmatrix} \hat{\mathbf{H}}_e & \hat{\mathbf{W}}(t) \\ \hat{\mathbf{W}}(t) & \hat{\mathbf{H}}_g \end{pmatrix}, \tag{2.5}$$

where $\hat{\mathbf{H}}_{g/e} = \hat{\mathbf{P}}^2/2\mu + \hat{\mathbf{V}}_{g/e}$ are the surface Hamiltonians, $\hat{\mathbf{P}}_{g/e}$ are the projections on the ground or excited electronic surface, $\hat{\mathbf{S}}_x$ is the transition operator in a two-level-system description of the electronic state, $\mu = m/2$ is the reduced mass of a diatomic molecule, and $\hat{\mathbf{V}}_g(R)$ and $\hat{\mathbf{V}}_e(R)$ are the electronic potential-energy surfaces of the ground and excited state. $\mathbf{W}(t)$ is the coupling between electronic states mediated by the electromagnetic field, which is described semiclassically in the dipole approximation by the following expression:

$$\hat{\mathbf{W}}(t) = -\tfrac{1}{2}\vec{\mathbf{D}} \cdot \vec{E}(t) = -\tfrac{1}{2}\mathbf{D} E(t)(e^{-i\omega t} + e^{i\omega t}), \tag{2.6}$$

where $\vec{\mathbf{D}}$ is the electronic transition dipole operator and $\vec{E}(t)$ is the linearly polarized electromagnetic field with a slowly varying envelope function $E(t)$ and the carrier frequency ω. Employing the rotating-wave approximation, an effective Hamiltonian operator is defined as

$$\tilde{\mathbf{H}} = \begin{pmatrix} \hat{\mathbf{H}}_e - \hbar\omega/2 & -E(t)\hat{\mathbf{D}}/2 \\ -E(t)\hat{\mathbf{D}}/2 & \hat{\mathbf{H}}_g + \hbar\omega/2 \end{pmatrix}, \tag{2.7}$$

where $\hat{\mathbf{D}} = \hat{\mathbf{D}}(\mathbf{R})$ is a scalar function of R. The dynamics of the photoassociation process is then described by solving the two-surface time-dependent Schrödinger equation generated by the effective Hamiltonian:

$$i\hbar \frac{\partial}{\partial t} \begin{pmatrix} \tilde{\psi}_e \\ \tilde{\psi}_g \end{pmatrix} = \tilde{\mathbf{H}} \begin{pmatrix} \tilde{\psi}_e \\ \tilde{\psi}_g \end{pmatrix}. \tag{2.8}$$

The vector $|\tilde{\psi}\rangle$ is related to the original state by the transformation

$$|\tilde{\psi}\rangle = e^{i\omega t \hat{\mathbf{S}}_z} |\psi\rangle, \tag{2.9}$$

TABLE II. The typical values of the propagation parameters.

Parameters	Typical value	Units
Grid spacing	0.05	a.u.
Number of grid points	16 384	
Time step	2	ps
Number of time steps	200	
Pulse duration	75	ps
Typical maximal Rabi frequency	10^{-6}	a.u.
Width of the initial wave packet	85	a.u.
Initial position of the wave packet	500	a.u.

where $\hat{\mathbf{S}}_z$ is the rotation generator given by the Pauli matrix σ_z multiplied by $\frac{1}{2}$.

The time dependency of the field frequency in the case of chirped pulse excitation is of the same character as the time dependency of the field envelope. Both are slowly varying functions of time compared to the time scale given by the field frequency itself and therefore allow application of the rotating-wave-approximation framework.

C. Numerical methods

To gain insight into the process, a numerical scheme to solve the time-dependent Schödinger equation is employed. The numerical results are converged to the accuracy of the computer that allows the evaluation of the approximations involved. It should be noted that there is no approximation used for the solution of the TDSE itself, which is (numerically) exact. The approximations used are related to the model, for instance the Born-Oppenheimer electronic potentials, the semiclassical electromagnetic field, and the dipole approximation. The method is based on the Fourier grid representation of the wave function [42]. An initial wave function is propagated in time using a Chebyshev polynomial expansion of the evolution operator [43]. The propagation was realized in discrete steps with a time increment shorter by two orders of magnitude than the pulse duration. The typical computation parameters, summarized in Table II, were chosen according to several criteria. The correct representation of the wave packet in a coordinate as well as a momentum representation dictated the grid parameters. The pulse characteristics correspond with both the experimental feasibility and the physical aspects of the photoassociation process.

III. LIGHT INDUCED POPULATION TRANSFER

There are two asymptotic limits to photoassociation, depending on the time scales of the dynamical processes involved. Those are determined by either the wave-packet motion or the excitation pulse duration. To gain insight into the process of excitation by a chirped pulsed field, the asymptotic cases are analyzed.

A. Continuous-wave case

The first limiting situation considered is continuous-wave (CW) light-induced population transfer between two molecular electronic states. For the CW excitation, the time scale is determined by the wave-packet motion. In the dressed potential picture, the excited surface crosses the ground-state potential at the point of resonance: $V_e(R_c)-\hbar\omega_0=V_g(R_c)$, as can be seen in Fig. 2. The process is then described by a Landau-Zener type of transition [44–47]. The coupling between the surfaces W is radiative and constant in time. For weak excitation fields, the interaction region is very small. The time scale of the process is then determined by the time for which a wave packet with an average velocity $\overline{v}=\langle\hat{\mathbf{P}}\rangle/\mu$ passes through the crossing point, Fig. 2.

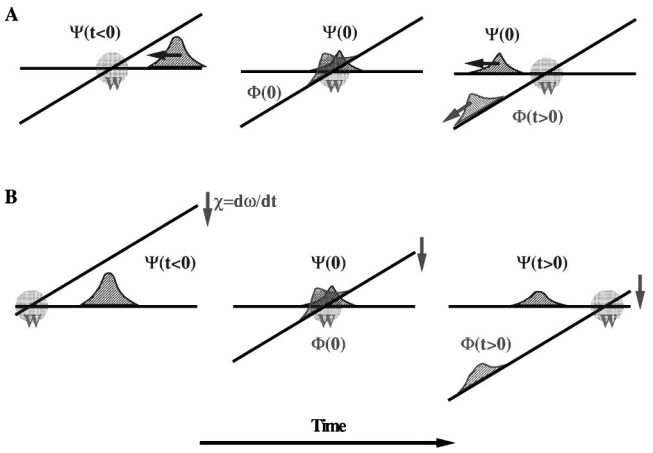

FIG. 2. A Landau-Zener picture of photoassociation on dressed potentials (top) where a wave packet moves through the crossing point located at the internuclear distance R_c. The dressed-state picture of the evolution of a wave packet on two potential surfaces coupled by chirped field (bottom), i.e., a frequency sweeps through the range given by the pulse bandwidth. The crossing point R_c is now determined by the instantaneous detuning.

To make the connection to the pulsed case clearer, one can think of the wave packet as stationary and the crossing potentials as moving toward the wave packet. Such a situation is equivalent to the excitation by a suitably chirped pulse. The difference between the potentials, which is equivalent to the rate the detuning is changing with time, is

$$\frac{1}{\hbar}\Delta(t)=t/\chi'=|F_e-F_g|\overline{v}t, \tag{3.1}$$

where $\Delta(t)$ is the detuning [see Eq. (3.3)], χ' is the linear chirp rate in frequency representation (see Appendix A), and F_i is the force or slope of surface i, i.e., $F_i=-\partial V_i/\partial R$. The wave packets in Fig. 2 represent a time-dependent numerical solution of the Schrödinger equation.

For the CW case, the radiative coupling $\hat{\mathbf{W}}$ is constant, leading to the probability of transition [44–46]:

$$P_{ge}\approx 1-e^{-2\pi\alpha^2}, \tag{3.2}$$

where $\alpha=|W|/\sqrt{|F_e-F_g|\overline{v}}$. When the adiabatic parameter $1/\alpha$ is small, the population transfer becomes complete. For instance, for the detuning corresponding to $R_c=100$ Å, thermal velocity at a temperature of 200 μK, and the CW field

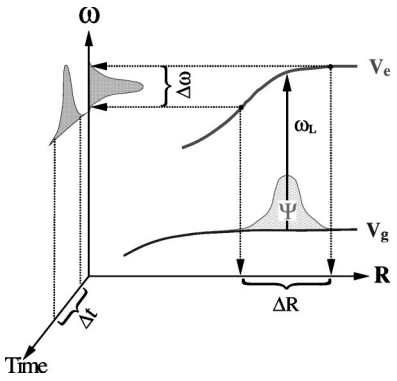

FIG. 3. The initial wave packet superimposed on ground potential surfaces. The reflection of the ground surface wave function on the excited electronic potential, i.e., the Frank-Condon principle, determines the minimal frequency bandwidth of the pulse. Such a pulse will excite simultaneously all the initial wave function. Its frequency spread is translated into a transform-limited pulse in the time domain.

intensity of 60 W/cm^2, the value of α is 4.2. Hence, the Landau-Zener picture provides a consistent conceptual framework.

B. Transform-limited pulsed field

A pulsed excitation of a slowly moving wave packet constitutes the case when the time scale of a population transfer is determined by the pulse duration. Insight into the photoassociation process and its manipulation can be gained by understanding the relation between the coupled nuclear and electronic dynamics and the dynamics of a two-level system (TLS). Using the fact that in cold collisions the nuclear motion is approximately stationary on the time scale of pulsed field excitation, a coordinate-dependent TLS is identified [48]. The optical pumping is spread over the range of coordinates which support the nuclear wave packet, as can be observed in Fig. 3.

At this point one has to identify the parameters of the coordinate-dependent TLS. As can be seen in Fig. 3, the detuning depends on the internuclear coordinate R,

$$\frac{1}{\hbar}\Delta(R)=\omega_0=\frac{1}{\hbar}\{[V_e(\infty)-V_g(\infty)]-\omega_L\}, \qquad (3.3)$$

where ω_L is the central frequency of the laser. Using the reflection principle (Fig. 3), the intensity at a particular coordinate location corresponds to the pulse intensity at a particular instantaneous frequency as this one correlates with the coordinate-dependent detuning.

The local coupling constant W is given by the instantaneous field of the pulse $E(\omega(R),t)$ mapped onto the internuclear distance using the reflection principle, and by the local transition dipole moment $\mu(R)$:

$$W(R)=E(\omega(R),t)\mu(R). \qquad (3.4)$$

The Rabi frequency becomes a function of position:

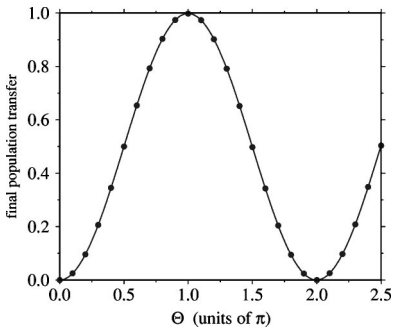

FIG. 4. The total population transfer $\langle\tilde{\psi}_e(t=\infty)|\tilde{\psi}_e(t=\infty)\rangle$, as a function of the integral of the Rabi frequency in the units of π. A wave packet of the Gaussian shape is promoted from a flat ground state onto an excited potential which linearly changes with distance. The Gaussian pulse coincides with the initial distribution of the population. The wave-packet dynamics is effectively frozen on the time scale of the interaction. The Rabi frequency function is modified by changing the intensity while keeping the pulse duration and hence the spectral bandwidth constant.

$$\Omega(R)=\sqrt{\Delta(R)^2+W(R)^2}. \qquad (3.5)$$

For sufficiently intense pulses, $E^2\gg\Delta^2$, the Rabi frequency becomes coordinate-independent. For these conditions, the wave packet will rotate intact to the upper electronic surface by an angle $\Theta=\int_{-\infty}^{t}\Omega(t')dt'$:

$$\tilde{\psi}_e(R,t)=\tilde{\psi}_g(R,-\infty)\sin(\Theta). \qquad (3.6)$$

To emphasize this point, a pulse in the frequency domain was created using the inversion principle. This pulse was then transformed into the time domain and used in the photoassociation simulation with different peak intensities. The total population transfer is shown in Fig. 4 exhibiting almost perfect Rabi oscillations. The population inversion, i.e., the complete population transfer, is achieved when θ is equal to π or its odd integral multiple as directed by the Rabi formula [49]. We call this the π pulse condition.

This model demonstrates that a wave function distributed in coordinate space effectively behaves as a single driven two-level system. For this system, the π pulse condition for complete population inversion exists.

C. Chirped pulsed field

The drawback of the π pulse method is that it is sensitive to the laser intensity and pulse duration. For a particular pair of atoms, the radiation coupling is weighted by $\cos^2\theta$, where θ is the angle between the electric-field direction and the internuclear axis. For an ensemble of nonoriented molecules, the π pulse condition cannot be obtained for all particles. Moreover, in the case of coupling of two potential curves of different topology, the definition of the π pulse is complicated, as addressed in the preceding section. These problems have been overcome in the TLS using adiabatic following techniques [34,35]. Experimentally, the easiest way to achieve adiabatic following is to sweep the frequency through the transition, i.e., create a chirped pulse.

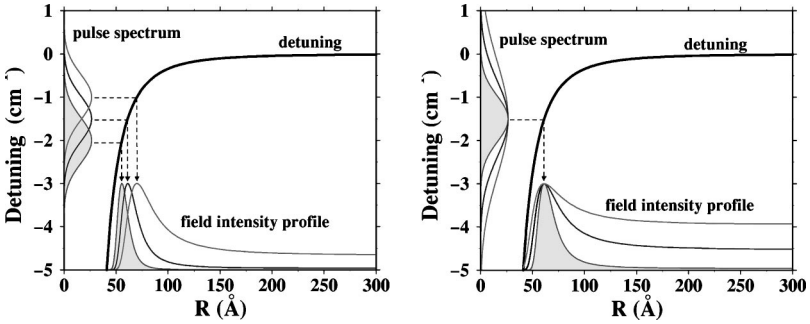

FIG. 5. The detuning as a function of the interatomic distance shown together with the pulse spectrum and its mapping onto the coordinate. Left: pulses with a width of 10 psec and different carrier frequencies. Right: pulses with widths corresponding to 5, 7, and 10 psec.

The adiabatic passage in a two-level system is symmetric to the chirp direction. In the present case, this symmetry is broken due to nuclear motion. One can distinguish the cases of population inversion [33] or a pump-dump process [28,33]. Both phenomena, mutually opposite, reduce to adiabatic following in the limit of infinitely slow wave-packet dynamics on the excitation time scale. The photoassociation process belongs to this category.

The nature and properties of the chirped pulse are presented in detail in Appendix A.

D. Adiabatic following

When the precession motion of a TLS is fast relative to the change of the axis of precession, the polarization axis follows the precession. Since the stationary photoassociating pair can be manipulated as a two-level system, the adiabatic following ideas can be employed in a straightforward way [29,34,35].

This leads again to the Landau-Zener model described by Eq. (3.2) for each internuclear distance R with a modified adiabatic parameter:

$$\frac{1}{\alpha^2} = \frac{|1/\chi'|}{|W(R)|^2}, \tag{3.7}$$

where χ' is the linear chirp rate in frequency representation (see Appendix A). As before, when $1/\alpha$ is small the adiabatic transfer is complete. Moreover, these conditions can be fulfilled for a large range of internuclear distances.

Figures 6 and 7 demonstrate complete population transfer for the Cs_2 photoassociation when a chirped pulse is employed. Once the π pulse condition is satisfied, the population inversion is achieved and the transfer is complete and robust provided the chirp rate is sufficiently large to fulfill adiabaticity. The efficiency is invariant with local changes of the transition dipole moment.

For the cold Cs_2 system, the direction of the chirp has no effect on the results. The efficiency of the population inversion is practically invariant to the chirp sign. For lighter systems which exhibit dynamics in a time scale comparable to the pulse duration, the symmetry between positive and negative chirp is broken. For a positive chirp, the population promoted onto the electronically excited potential moves in the opposite direction of the energy sweep. This new portion of the wave packet does not interfere with the previous portions leading to smooth and complete population transfer. For a negatively chirped pulse, the interference leads to a reduction in the process efficiency [33].

IV. PHOTOASSOCIATION OF CESIUM

The insight gained in Sec. III is applied to the specifics of the photoassociation reaction in the Cs_2. In particular, one would like to know if under realistic experimental constraints the process can be optimized.

A. Pulsed enhancement of photoassociation

A chirped pulsed excitation can lead to a complete population inversion. The task is therefore to identify the experimentally accessible control parameters of the pulse: the pulse central frequency ω_L, the pulse spectral width $\Gamma = 1/\tau$, and the chirp rate χ. Figure 5 shows the relation between the detuning of the central frequency of the laser and the position of the local TLS for the Cs_2.

Specifically for the $^3\Sigma_u^+$ to the 0_g^- transition of the Cs_2, the detuning Δ becomes

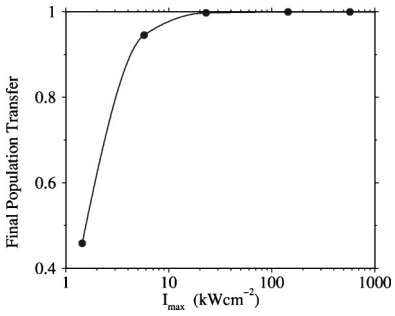

FIG. 6. The total population transfer as a function of the maximal intensity of the chirped pulse. Once the population inversion is achieved, further increase of the intensity does not lead to the Rabi cycling. The simulation was carried out using a pulse of the transform-limited duration 5 ps stretched to 75 ps by chirping ($\chi' = 374$ ps^2). The central frequency of the Gaussian pulse $\omega_L = 11\,732.16$ cm^{-1} ($\lambda = 852.357$ nm) results in the strongest coupling between the electronic potentials at the distance of 260 Å. The pulse bandwidth $\Gamma = 2.65$ cm^{-1} couples the ground and excited potential in a large range of internuclear distance which covers the entire area where the wave-packet population is nonvanishing. (The validity of the curve between the indicated points was tested.)

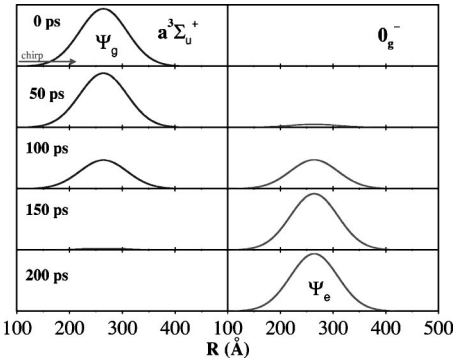

FIG. 7. The snapshots of the population transfer mediated by chirped pulsed field. The instantaneous coupling window moves from left to right, as indicated, promoting population adiabatically from the ground onto the excited electronic potential. The translation of the wave packet is negligible at the time scale of the excitation process. The top of the arrow marks the position where the coupling is maximal. That corresponds to the maximal intensity of the pulse reached at $t=100$ ps. The simulation parameters are identical to those of Fig. 6.

$$\Delta(R)=[V_{0_g^-}(R)-V_{0_g^-}(\infty)]-[V_{^3\Sigma_u^+}(R)-V_{^3\Sigma_u^+}(\infty)]$$

$$=-\frac{D_3}{R^3}+O(R^{-6}). \tag{4.1}$$

As can be seen, there is a wide choice of pulse parameters which will achieve complete population transfer in a limited coordinate range. For example, a pulsed field of central frequency $\omega_L=11\,732.16\ \mathrm{cm}^{-1}$ with bandwidth $\Gamma=2.65\ \mathrm{cm}^{-1}$ corresponding to a transform-limited pulse of 5 ps linearly chirped by a factor of 15 ($\chi'=374\ \mathrm{ps}^2$) is applied to the photoassociation of two ultracold cesium atoms. As shown in Fig. 6, complete population transfer is obtained along several orders of magnitude of the maximal field intensity.

The dynamics of the population transfer is illustrated by snapshots in Fig. 7. The motion of the wave packet on both potentials is negligible on the time scale of the excitation process. Therefore, the use of the negative chirp instead of the positive one has a negligible influence on the process efficiency ($\approx 0.1\%$).

The efficiency of the population inversion by a chirped field is limited by the adiabatic condition. Small chirp results in small redistribution of the spectral components of the pulse and its small prolongation. Consequently, its interaction with the system is too fast to keep the adiabaticity of the process. The increase of the field intensity above the inversion limit lowers the population transfer efficiency, as shown in Fig. 8.

B. The number of particles addressed by a laser pulse

The simulation demonstrates that complete population transfer by a chirped pulse is obtained for amplitude located between $R_{\min}$ and $R_{\max}$ provided the adiabatic condition is fulfilled, see Fig. 5. The coupling range is determined by the central frequency of the pulse, its bandwidth Γ, and the energy difference between both coupled potentials. This defines an active spherical shell for each atom in a three-dimensional cloud. Its extent can be tuned by changing the pulse parameters, see Fig. 9.

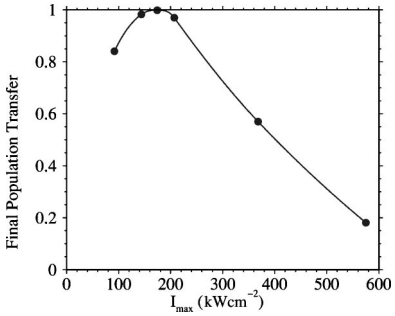

FIG. 8. The breakdown of the adiabaticity of the process. A too low chirp rate results in lowering the transfer efficiency with the field intensity. The parameters of the pulse are the same as in Fig. 6 except the chirp rate which now stretches the pulse by a factor of 3 ($\chi'=71\ \mathrm{ps}^2$).

The shell volume

$$\mathcal{V}_{\mathrm{pa}}=\frac{4\pi}{3}(R_{\max}^3-R_{\min}^3) \tag{4.2}$$

multiplied by the particle density gives an estimate of the number of pairs transferred onto the excited electronic state,

$$N_{\mathrm{pa}}=(\mathcal{V}_{\mathrm{pa}}n)\mathcal{V}n/2\eta_p, \tag{4.3}$$

where $\mathcal{V}$ is the trap volume addressed by a photoassociation laser beam, n is the particle density, and η_p is the population transfer efficiency factor.

In the case of cesium photoassociation, the shell volume is conveniently expressed using the carrier frequency and bandwidth of the pulsed field. Since the topology of the difference potential is $-D_3/R^3$, up to the negligible factor $O(1/R^6)$, the volume becomes

$$\mathcal{V}_{\mathrm{pa}}=\frac{8\pi D_3}{3\hbar}\frac{\Gamma}{\Delta_0^2-\Gamma^2}, \tag{4.4}$$

where Δ_0 is the difference between the carrier frequency of the field and the difference potential at the infinite separa-

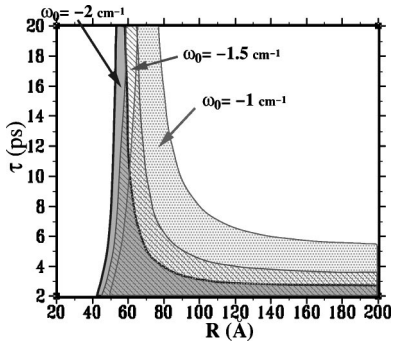

FIG. 9. The coordinate range addressed by pulses of different detuning ω_0 and duration τ.

tion, i.e., the absolute value of the detuning of the carrier frequency. For small detuning values and broadband pulses, the coordinate range of the pulse becomes infinite. As will be seen later, photoassociation at large interatomic distances does not lead to molecular production because the excited pair will decay much before any interaction takes place.

Repetition rate consideration

The repetition rate of the laser is limited by the time needed for the reconstruction of the particle distribution perturbed by a laser pulse. There are two mechanisms for filling in the dynamical hole created in the ground-state density by the excitation. The first is due to the thermal motion and the second is due to quantum uncertainty spreading. To optimize molecular formation, the rate of these mechanisms has to be faster than the rate of spontaneous emission.

The thermal velocity filling rate is determined by the mean relative velocity $\overline{v}$ of particles and by the range of interatomic distance $\Delta R=\frac{1}{2}(R_{\max}-R_{\min})$ for which the distribution was perturbed:

$$\kappa_T=\frac{\overline{v}}{2\Delta R}. \tag{4.5}$$

The spontaneous-emission process presents a natural upper bound for the extension of the size of the overall coupling window. The longer the interatomic distance at which cesium atoms are excited, the higher the probability of the decay off the molecular bound levels. Hence, the repetition rate is set equal to the spontaneous-emission rate of 30 ns. That implies $\Delta R\approx 75$ Å.

The quantum uncertainty filling rate is determined by the velocity $\overline{v_q}\approx\hbar/(\mu\Delta R)$, where μ is the relative mass of the colliding pair. This leads to the relation

$$\kappa_q\approx\frac{\overline{v_q}}{2\Delta R}=\frac{\hbar}{8\mu\Delta R^2}. \tag{4.6}$$

For impulsive conditions to prevail the quantum filling time scale has to be much larger than the pulse duration. For $\Delta R=75$ Å, it is 120 ns, which easily fulfills this requirement. When the quantum rate κ_q becomes comparable to the thermal rate κ_T, the distinction between a CW and a pulsed excitation diminishes.

We now compare the photoassociation rate of the CW excitation with the rate of the pulsed excitation at this repetition rate. The maximal cross section for the CW case is $\sigma\approx 4\pi R_c^2$, where R_c is the crossing point. The rate becomes

$$k_{\rm cw}=(\sigma\overline{v}n)(n\mathcal{V}/2)\,\eta_{\rm cw}=2\pi R_c^2\mathcal{V}n^2\overline{v}\,\eta_{\rm cw} \tag{4.7}$$

for the pulsed case,

$$k_p=(\mathcal{V}_{\rm pa}n)\,\kappa(\mathcal{V}n/2)\,\eta_p=\tfrac{1}{4}(\mathcal{V}_{\rm pa}\mathcal{V}n^2\overline{v}/\Delta R)\,\eta_p. \tag{4.8}$$

The ratio between these terms becomes:

$$\frac{k_{\rm cw}}{k_p}=\frac{8\pi R_c^2}{\mathcal{V}_{\rm pa}\Delta R}\,\frac{\eta_{cw}}{\eta_p}. \tag{4.9}$$

Due to the Rabi cycling of population between the ground and excited state in the case of CW field photoassociation, the theoretically maximal value of the population transfer efficiency $\eta_{\rm cw}$ is 0.5. On the other hand, η_p is equal to unity, reflecting the population inversion due to the adiabatic following by a chirped field. Taking this into account and evaluating $\mathcal{V}_{\rm pa}$ around the center of the coordinate range addressed by the pulsed field coinciding with R_c, the ratio between the two rates becomes

$$\frac{k_p}{k_{cw}}=2\left(1+\frac{1}{3}\,\frac{\Delta R^2}{R_c^2}\right). \tag{4.10}$$

Therefore, if the condition of the adiabatic following by the chirped field is fulfilled, then the corresponding photoassociation process is at least twice as efficient as that mediated by the CW field.

V. COLD-MOLECULE FORMATION

The photoassociation of a pair of atoms into the 0_g^- electronic surface is only the first step in the formation of cold molecules. The crucial second step is spontaneous emission into the well of the $^3\Sigma_u^+$ potential. Only part of the pair of photoassociated atoms decays back to the ground electronic state and forms a stable molecule. For this to happen, the emitted photon has to have larger energy than the asymptotic atomic excitation energy. This defines a small window of internuclear distances within which the colliding pair has to enter. If the photoassociation process occurs at a large internuclear distance, most likely the pair of atoms will decay before reaching the molecular forming window. If the photoassociation point is too short, the molecule will reach the inner turning point of the outer well of the excited 0_g^- potential and will reflect back before reaching the molecular forming window.

The rate of spontaneous decay at a particular internuclear distance R becomes [50]

$$k_{eg}(R)=\frac{4}{3\hbar c^3}[\omega_\infty+\Delta(R)]^3\mu(R)^2, \tag{5.1}$$

where $\omega_\infty+\Delta(R)$ is the Bohr frequency for the electronic potentials at a given value of R, $\mu(R)$ is the coordinate-dependent dipole moment, and c is the speed of light.

Figure 10 shows the spontaneous-emission decay rate as a function of internuclear distance. One can observe a clear enhancement of the rate of spontaneous emission at distances corresponding to molecular production. This rate is further enhanced due to the slowing down of the excited pair of atoms close to the inner turning point of the outer potential well. As a result, the system spends more time at these internuclear configurations.

An estimate of the fraction of cold molecules formed is carried out by propagating the newly created excited-state

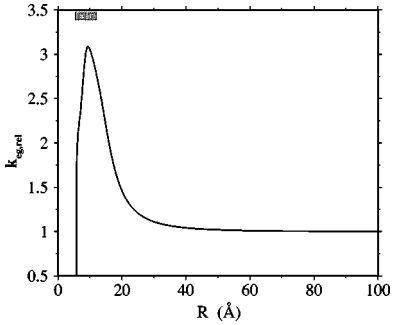

FIG. 10. The spontaneous-emission rate of circularly polarized light vs the internuclear distance. The plot shows a high probability of spontaneous decay at distances corresponding to the bound levels of the electronic ground state (indicated by the box). The rate is renormalized to unity at the infinite atomic separation.

wave function. The amplitude loss due to spontaneous emission is described by an optical potential with the shape determined by Eq. (5.1):

$$iV_{\mathrm{opt}} = \sqrt{k[\omega_\infty + \Delta(R)]^3 \mu(R)^2}. \tag{5.2}$$

The decay to different regions of the internuclear distance is accumulated in time leading to the fraction of photoassociated molecules that result in cold molecules in the $^3\Sigma_u^+$ state. By this procedure, the loss terms leading to the formation of hot atoms are accounted for.

Complete simulation of the cold-molecule formation including photoassociation as well as spontaneous decay for both types of field was carried out. It revealed that the efficiency of the production of a cold cesium dimer is higher approximately by a factor of 3 in the case of chirped pulse photoassociation on the time scale of spontaneous emission compared to the CW scheme. The crossing point of the CW dressed potentials is located at the internuclear distance of 100 Å coinciding with the maximal probability density of the wave packet. Due to the fact that the excitation by a chirped field is more delocalized, starting at 100 Å and terminating at the infinite separation, we chose 300 Å as the initial wave-packet mean position; the field is maximized at this point. This results in the spread of the excited population along a larger range of the coordinate, which consequently biases the pulsed case in favor of the CW one. The result is illustrated in Fig. 11.

Further optimization of cold-molecule formation is possible in both the CW and pulses excitation. This was not attempted in the present study.

The previous consideration opens also the question of the angular momentum of the colliding cesium atoms. The potential barrier due to the nonzero angular momentum is significant at the ground state at the distance of 50 Å and basically prevents a non-negligible part of the population to get to a shorter internuclear distance. Then the ground-state collisional events consist exclusively of the *s* waves. The situation of the excited state is completely different. Since the gradient of the potential is very high, the effect of the angular momentum is negligible and colliding particles are attracted to each other even if their angular momentum reaches

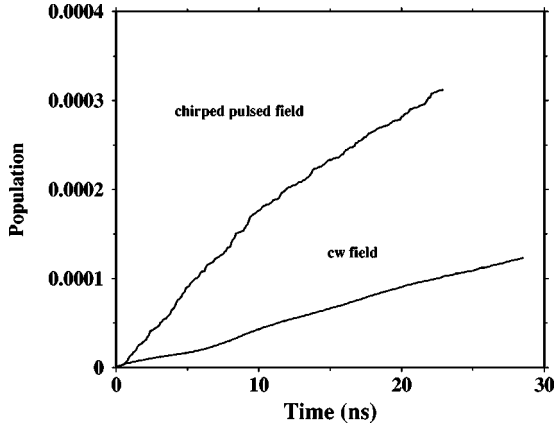

FIG. 11. The population transfer to cold-molecular states due to the spontaneous decay.

high values. Therefore, the photoassociation, particularly that using the complete population inversion, leads to a considerable and observable portion of molecules formated with high angular momentum [51,52].

The application of a pulsed electromagnetic field addresses potential curves in a large range of energies compared to the CW case. This necessarily raises the issue of the selectivity of the excitation process at long range when the hyperfine levels are converging to the asymptotic atomic state. One can expect partial population transfer to many attractive hyperfine levels which are approaching the target potential from below if positive chirp is applied. This behavior can become significant at large internuclear separation. We do not expect a strong impact on the cold-molecule formation, whose efficiency is mostly determined by photoassociation at intermediate distances of up to several hundreds of atomic units.

VI. DISCUSSION

The present work is part of a growing trend to study photoassociation in the time domain [24–26,53–55,60]. This framework enables us to gain insight into the use of a simple coherent control manipulation, which was the purpose of this study. The photoassociation route to cold molecules depends on two factors. The first is the rate of the photoassociation process and the second is the formation of stable molecules through spontaneous emission. Ideas emerging from the field of coherent control can address both steps. The results of the analysis presented in this paper show that the first step is completely controllable, leading to 100% photoassociation yield for pairs of atoms in a preassigned window of internuclear distances. The time-dependent control method relies on a simple chirp of pulses in the picosecond regime. The population transfer to the excited electronic surface leaves a void on the ground surface. Filling this void becomes the rate-limiting step in the formation of cold molecules. The competition between a thermal and a quantum process determines this rate.

Control of the second step of cold-molecule formation is more involved. It requires a Frank-Condon window from the excited to ground electronic surface. Enhancement of this

step is possible by focusing the photoassociated wave packet on this region. For a CW field, there are two experimentally attainable control knobs: detuning and intensity. For the pulsed excitation considered here, there are two additional control knobs: the pulse duration and the chirp. This means that there are more opportunities for optimizing the process. Recent studies show that the photoassociation yield is extremely sensitive to the shape of the potentials at the hump separating the inner and outer wells of the 0_g^- potential [36]. The emphasis in this study was not on this step. To do so requires very detailed knowledge of the potential at the Frank-Condon region. More sophisticated control mechanisms are possible, relying on complete control of the pulse shape that can be implemented by feedback [27]. Another possibility is control of direct photoassociation to a specific bound vibrational level [56] from the continuum.

Another consideration is the demonstrated ability to trap the molecules formed by the photoassociation process [57]. On the trapped molecules, further manipulations can be performed, for example optical cooling of the internal degrees of freedom of the molecule [8,58,59]. To conclude, this study is a first step in illuminating the practical possibilities of coherent manipulations in cold-molecule formation.

ACKNOWLEDGMENTS

Part of the research was carried out in the Laboratoire Aimé Cotton of the CNRS in Orsay, France, in the framework of the Arc-en-Ciel/Keshet Project. The work was supported by the Israel Science Foundation (Moked). We are indebted to these institutions for providing a creative atmosphere for scientific work. The Fritz Haber Research Center was supported by the Minerva Gesellschaft für die Forschung, GmbH München, FRG. We express our acknowledgment to Dr. Viaceslav Kokoouline for his kind help with the application of the Fourier Grid Method for the calculation of the initial atomic distribution. Jiri Vala thanks the People of the Supercomputing Center Brno, Czech Republic, and, in particular, Dr. Ludek Matyska for the access to their supercomputer facilities, on which a part of the work was performed.

APPENDIX: CHIRPED PULSED FIELD

We consider only the linear chirp following Band [29] and Cao [33]. Using a Gaussian pulse envelope, we express the chirped electromagnetic field in a frequency representation with the following form:

$$\tilde{E}(\omega)=\tilde{E}(\omega_0)\exp\left(-\frac{(\omega-\omega_0)^2}{2\Gamma^2}-i\chi'\frac{(\omega-\omega_0)^2}{2}\right), \tag{A1}$$

where ω_0 is the transform-limited carrier frequency of the field, Γ is the spectral bandwidth of the pulse, and χ' is the chirp rate in energy representation given by $dt/d\omega$. The chirp rate term causes a phase shift of each spectral component of the field proportional to its ''distance'' from the carrier frequency. The field in time representation is given by its Fourier transform,

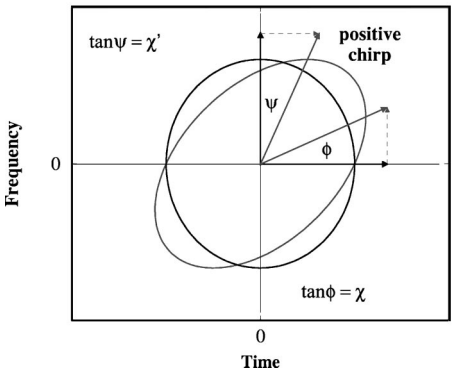

FIG. 12. The effect of linear dispersive media on a transform-limited pulse in the Husimi plot. The meaning of the chirp rate in the energy representation as a mutual displacement of the spectral components of the pulse in time is illustrated together with its time-domain counterpart.

$$E(t)=E_0\exp\left(-\frac{t^2}{2\tau^2}-i\omega_0 t-i\chi\frac{t^2}{2}\right), \tag{A2}$$

where χ is the linear chirp rate in time representation $d\omega/dt$. Chirp results in a prolongation of the pulse in the time domain [33] reducing the local field intensity to conserve the total pulse energy

$$\tau^2=\frac{1}{\Gamma^2}+\Gamma^2\chi'^2. \tag{A3}$$

Time and frequency representations of the chirp rate are then related by the following formula:

$$\chi=\frac{\Gamma^2}{\tau^2}\chi'. \tag{A4}$$

Chirp is obtained by propagation of a transform-limited pulse through a dispersive medium. During this process, each of the spectral components of the pulse gains a certain phase shift given by the specific value of the frequency-dependent group velocity $v_g(\omega)$. This results in a mutual displacement of the spectral components in the time domain. If the displacement is a linear increasing or decreasing function of frequency, we talk about linear positive or negative chirp, respectively. An example of a positively chirped pulse visualized using the Husimi plot is shown in Fig. 12. Chirping of a pulse does conserve its bandwidth and total power.

To establish a relation between linear chirp rate in an energy representation and properties of the dispersive media, namely the width of the dispersive slab L and the group velocity dispersion $w=-[1/v_g(\omega_0)^2]dv_g(\omega)/d\omega$, we expand the group velocity around the carrier frequency using the Taylor expansion,

$$v_g(\omega)=v_g(\omega_0)-v_g(\omega_0)^2 w\Delta\omega, \tag{A5}$$

where $\Delta\omega=(\omega-\omega_0)$. Time delay of a spectral component of the pulse divided by $\Delta\omega$ gives the chirp rate in the energy representation,

$$\chi' = \frac{\Delta t}{\Delta\omega} = \frac{Lw}{1-v_g(\omega_0)w\Delta\omega}. \tag{A6}$$

The second term in the denominator, which makes the chirp rate frequency-dependent, comes from the difference in time of remaining in the dispersive media of the width L for a different spectral component of the pulse. A value of this term is very small, i.e., typically of the order of 10^{-5}, and hence does not break linearity of the chirp rate significantly. For this reason, the chirp rate can reliably be approximated by the product Lw. The concept of chirp rate as the effect of dispersive media is graphically illustrated in Fig. 12.

[1] H. R. Thorsheim, J. Weiner, and P. S. Julienne, Phys. Rev. Lett. **58**, 2420 (1987).

[2] P. D. Lett, K. Helmerson, W. D. Philips, L. P. Ratliff, S. L. Rolston, and M. E. Wagshul, Phys. Rev. Lett. **71**, 2200 (1993).

[3] V. Bagnato, L. Marcassa, C. Tsao, Y. Wang, and J. Weiner, Phys. Rev. Lett. **70**, 3225 (1993).

[4] P. A. Molenaar and P. Van der Straten, Phys. Rev. Lett. **77**, 1460 (1996).

[5] J. D. Miller, R. A. Cline, and D. J. Heinzen, Phys. Rev. Lett. **71**, 2204 (1993).

[6] D. Leonhardt and J. Weiner, Phys. Rev. A **52**, R4332 (1995).

[7] E. R. I. Abraham, N. W. M. Ritchie, W. I. McAlexander, and R. G. Hulet, J. Chem. Phys. **103**, 7773 (1995).

[8] H. Wang, P. L. Gould, and W.C. Stwalley, Phys. Rev. A **53**, R1216 (1996).

[9] A. Fioretti, D. Comparat, A. Crubellier, O. Dulieu, F. Masnou-Seeuws, and P. Pillet, Phys. Rev. Lett. **80**, 4402 (1998).

[10] A. Fioretti, D. Comparat, C. Drag, C. Amiot, O. Dulieu, F. Masnou-Seeuws, and P. Pillet, Eur. Phys. J. D **5**, 389 (1999).

[11] N. Herschbach, P. J. J. Tol, W. Vassen, W. Hogervorst, G. Woestenek, J. W. Thomsen, P. van der Straten, and A. Niehaus, Phys. Rev. Lett. **84**, 1874 (2000).

[12] A. P. Mosk, M. W. Reynolds, T. W. Hijmans, and J. T. M. Walraven, Phys. Rev. Lett. **82**, 307 (1999).

[13] J. P. Shaffer, W. Chalupezak, and N. P. Bigelow, Phys. Rev. Lett. **82**, 1124 (1999).

[14] U. Schloder, H. Engler, U. Schunemann, R. Grimm, and M. Weidemuller, Eur. Phys. J. D **7**, 331 (1999).

[15] N. Nikolov, E. E. Eyler, X.T. Wang, J. Li, H. Wang, W. C. Stwalley, and Ph. Gould, Phys. Rev. Lett. **82**, 703 (1999).

[16] C. Gabbanini, A. Fioretti, A. Lucchesini, S. Gozzini, and M. Mazzoni, Phys. Rev. Lett. **84**, 2814 (2000).

[17] R. Napolitano, J. Weiner, C. J. Williams, and P. S. Julienne, Phys. Rev. Lett. **73**, 1352 (1994).

[18] P. S. Julienne, J. Res. Natl. Inst. Stand. Technol. **101**, 487 (1996).

[19] P. Pillet, A. Crubellier, A. Bleton, O. Dulieu, P. Nosbaum, I. Mourachko, and F. Masnou-Seeuws, J. Phys. B **30**, 2801 (1997).

[20] R. Côté and A. Dalgarno, Phys. Rev. A **58**, 498 (1998).

[21] R. Côté, A. Dalgarno, Y. Sun, and R. G. Hulet, Phys. Rev. Lett. **74**, 3581 (1995).

[22] C. Drag, B. L. Torla, O. Dulieu, D. Comparat, M. Vatasescu, S. Boussen, S. Guibal, A. Crubellier, and P. Pillet, IEEE J. Quantum Electron. (to be published).

[23] M. Mackie and J. Javanainen, Phys. Rev. A **60**, 3174 (1999).

[24] U. Marvert and M. Dantus, Chem. Phys. Lett. **245**, 8013 (1995).

[25] P. Gross and M. Dantus, J. Chem. Phys. **106**, 8013 (1997).

[26] P. Backhaus, B. Schmidt, and M. Dantus, Chem. Phys. Lett. **306**, 18 (1999).

[27] A. Assion, T. Baumert, M. Bergt, T. Brixner, B. Kiefer, V. Seyfried, M. Strehle, and G. Gerber, Science **282**, 919 (1998).

[28] S. Ruhman and R. Kosloff, J. Opt. Soc. Am. B **7**, 1748 (1990).

[29] Y. B. Band and O. Magnes, Phys. Rev. A **50**, 584 (1994).

[30] C. J. Bardeen, Q. Wang, and C. V. Shank, Phys. Rev. Lett. **75**, 3410 (1995).

[31] K. Mishima and K. Yamashita, J. Chem. Phys. **110**, 7756 (1999).

[32] I. R. Sola, V. S. Malinovsky, B. Y. Chang, J. Santamaria, and K. Bergmann, Phys. Rev. A **59**, 4494 (1999).

[33] J. Cao, Ch. J. Bardeen, and K. R. Wilson, Phys. Rev. Lett. **80**, 1406 (1998).

[34] L. Allen and J.H. Eberly, *Optical Resonance and Two-Level Atoms* (Dover Publications, Inc., New York, 1987).

[35] J.H. Eberly, Opt. Express **4**, 217 (1999).

[36] M. Vatasescu, O. Dulieu, C. Amiot, D. Comparat, C. Drag, V. Kokouline, F. Masnou-Seeuws, and P. Pillet, Phys. Rev. A **61**, 044701 (2000).

[37] N. Spiess, Ph.D. thesis, Fachbereich Chemie, Universität Kaiserlautern (1989).

[38] M. Marinescu and A. Dalgarno, Phys. Rev. A **52**, 311 (1995).

[39] A. Fioretti, D. Comparat, C. Drag, T. F. Gallagher, and P. Pillet, Phys. Rev. Lett. **82**, 1839 (1999).

[40] V. Kokoouline, O. Dulieu, R. Kosloff, and F. Masnou-Seeuws, J. Chem. Phys. **110**, 9865 (1999).

[41] V. Kokoouline, O. Dulieu, and F. Masnou-Seeuws, Phys. Rev. A **62**, 032716 (2000).

[42] R. Kosloff, *Quantum Molecular Dynamics on Grids*, in *Dynamics of Molecules and Chemical Reactions*, edited by R. E. Wyatt and J. Z. Zhang (Marcel Dekker, New York, 1996), pp. 185–230.

[43] R. Kosloff, Annu. Rev. Phys. Chem. **45**, 145 (1994).

[44] L. D. Landau, Z. Phys. Sov. **2**, 46 (1932).

[45] C. Zenner, Proc. R. Soc. London, Ser. A **137**, 696 (1932).

[46] N. V. Vitanov and K. S. Souminen, Phys. Rev. A **59**, 4580 (1999).

[47] C. Zhu and H. Nakamura, J. Chem. Phys. **102**, 7448 (1995).

[48] U. Banin, A. Bartana, S. Ruhman, and R. Kosloff, J. Chem. Phys. **101**, 8461 (1994).

[49] C. Cohen-Tannoudji, B. Diu, and F. Laloë, *Quantum Mechanics* (John Wiley, New York, 1977).

[50] G. C. Schatz and M. A. Ratner, *Quantum Mechanics in Chem-*

istry (Prentice-Hall International, Inc., Englewood Cliffs, NJ, 1993).
[51] S. D. Gensemer and P. L. Gould, Phys. Rev. Lett. **80**, 936 (1998).
[52] V. Sanchez-Villicana, S. D. Gensemer, and P. L. Gould, Phys. Rev. A **54**, R3730 (1996).
[53] M.V. Korolkov, J. Manz, G. K. Paramonov, and B. Schmidt, Chem. Phys. Lett. **260**, 604 (1996).
[54] H.M.J.M. Boesten, C. C. Tsai, B. J. Verhaar, and D. J. Heinzen, Phys. Rev. Lett. **77**, 5194 (1996).
[55] M. Mackholm, A. Giusti-Suzor, and F. H. Mies, Phys. Rev. A **50**, 5025 (1994).
[56] A. Vardi, D. Abrashkeevich, E. Frishman, and M. Shapiro, J. Chem. Phys. **107**, 6166 (1997).
[57] T. Takekoshi, B. M. Patterson, and R. J. Knize, Phys. Rev. Lett. **81**, 5105 (1998).
[58] A. Bartana, R. Kosloff, and D. J. Tannor, J. Chem. Phys. **99**, 196 (1993).
[59] A. Bartana, R. Kosloff, and D. J. Tannor, J. Chem. Phys. **106**, 1435 (1997).
[60] M. Vatasescu, O. Dulieu, R. Kosloff, and F. Masnou-Seeuws (unpublished).